SUPPORTING INFORMATION

Oxygen Recombination Probability Data for Plasma-Assisted Atomic Layer Deposition of SiO_2 and TiO_2

Karsten Arts[1], Sanne Deijkers,[1] Riikka L. Puurunen[2], Wilhelmus M.M. (Erwin) Kessels[1,a)] and Harm C.M. Knoops[1,3,a)]

[1]*Eindhoven University of Technology, P.O. Box 513, 5600 MB Eindhoven, The Netherlands*

[2]*Aalto University School of Chemical Engineering, P.O. Box 16100, FI-00076 AALTO, Finland*

[3]*Oxford Instruments Plasma Technology, North End, Bristol, BS49 4AP, United Kingdom*

a) Authors to whom correspondence should be addressed. Electronic mail: w.m.m.kessels@tue.nl and h.c.m.knoops@tue.nl

Abstract of corresponding article: Atomic layer deposition (ALD) can provide nm-thin films with excellent conformality on demanding 3D substrates. This also holds for plasma-assisted ALD, provided that the loss of reactive radicals through surface recombination is sufficiently low. In this work, we determine the surface recombination probability *r* of oxygen radicals during plasma ALD of SiO_2 and TiO_2 for substrate temperatures from 100 to ~240 °C and plasma pressures from 12 to 130 mTorr (for SiO_2). For both processes the determined values of *r* are very low, i.e., ~10^{-4} or lower, and decrease with temperature and pressure down to ~10^{-5} within the studied ranges. Accordingly, deposition on trench structures with aspect ratios (ARs) of <200 is typically not significantly limited by recombination and obtaining excellent film conformality is relatively facile. For higher AR values, e.g., approaching 1000, the plasma time needed to reach saturation increases exponentially and becomes increasingly dependent on the process conditions and corresponding value of *r*. Similar dependence on process conditions can be present for plasma ALD of other materials as well, where in certain cases film growth can already be recombination-limited for AR values of ~10. Radical recombination data and trends as provided by this work are valuable for optimizing plasma ALD throughput and feasibility for high-AR applications and can also serve as input for modelling of radical recombination mechanisms.

In this work, we studied film penetration into high-aspect-ratio (AR) structures during plasma-assisted atomic layer deposition (ALD) of SiO_2 and TiO_2, at different substrate temperatures and plasma pressures. The film penetration depths were related to the surface recombination probability r of the plasma radicals. In this document, we provide further details on the analytical model employed. Secondly, we provide additional experimental information and data, namely: 1) an overview of the measured thickness profiles used to determine the reported values of r, 2) the determined values of the parameter $t_{50\%}$, 3) the method used to calculate the reported uncertainties, and 4) experimental details regarding the transmission-electron-microscope image given in the introduction of this work.

MODELLING: Nomenclature

Here we give an overview of the used parameters and their definition. Note that in this work the provided equations are used to describe recombination-limited film growth during plasma ALD, in which case the "reactant" refers to the reactive plasma radicals (e.g., atomic O when growing an oxide).

A_0	Average surface area per adsorption site (m^2)
D	Diffusion coefficient of gas-phase reactant in high-AR structure ($m^2 \cdot s^{-1}$)
h	Gap height of lateral-high-aspect-ratio trench (m)
f	Dimensionless factor used in the correction $t_{50\%} = t_{50\%,planar}(1 + f)$ (-)
L	Length of high-aspect-ratio structure (m)
$n(z,t)$	Number density of gas-phase reactant species (m^{-3})
n_0	Number density of gas-phase reactant species at entrance of high-aspect-ratio structure (m^{-3})
$\theta(z,t)$	Surface coverage with $\theta = 1$ when being in saturation ($0 \leq \theta \leq 1$)
$PD^{50\%}$	Half-thickness-penetration-depth of deposited film (m)
r	Surface recombination probability ($0 \leq r \leq 1$)
s_0	Initial sticking probability ($0 \leq s_0 \leq 1$)
S	Surface area of high-aspect-ratio structure (m^2)
t	Dosing time of (co-)reactant (s)
$t_{50\%,planar}$	Dosing time needed for 50% saturation on a planar substrate (s)
$t_{50\%}$	Dosing time needed for 50% saturation, corrected for describing film penetration into a high-aspect-ratio structure during recombination-limited growth (s)
v_{th}	Average thermal velocity of gas-phase reactant species ($m \cdot s^{-1}$)
V	Volume of high-aspect-ratio structure (m^3)
z	Distance into high-aspect-ratio structure (m)

MODELLING: Derivation of the parameter $t_{50\%}$

In this work, an analytical relation was derived between the surface recombination probability r and the half-thickness-penetration-depth $PD^{50\%}$ of a film grown by plasma ALD into a high-AR structure. This relation was derived on the basis of the following reaction-diffusion model, which describes plasma ALD on a one-dimensional high-AR structure:[1,2]

$$\frac{\partial n}{\partial t} - D\frac{\partial^2 n}{\partial z^2} = -\frac{1}{4} n v_{th} \frac{S}{V}(s_0(1-\theta) + r) \quad \text{(S1)}$$

$$\frac{\mathrm{d}\theta}{\mathrm{d}t} = \frac{1}{4} n v_{th} A_0 s_0 (1-\theta) \quad \text{(S2)}$$

In the description of a plasma half-cycle, $n(z,t)$ represents the number density of gas-phase reactive radicals (m^{-3}), which have an initial sticking probability s_0 ($0 \leq s_0 \leq 1$) and a thermal velocity v_{th} (m/s). Furthermore, t denotes the (plasma) dosing time (s), $\theta(z,t)$ the surface coverage ($0 \leq \theta \leq 1$), A_0 the average surface area per adsorption site (m^2), z the distance into the high-AR structure (m), D the diffusion coefficient (m^2/s) and S/V the surface to volume ratio of the structure (m^{-1}).

For a trench with gap height h and width $w \gg h$, the surface to volume ratio equals $\frac{S}{V} = \frac{2(wL+hL)}{whL} \approx \frac{2wL}{whL} = \frac{2}{h}$ (see Figure S1). Moreover, in the Knudsen approximation for molecular flow, the diffusion coefficient is calculated as $D = \frac{2}{3} v_{th} h$.[3,4] Similarly, for a circular pore with diameter d, the surface to volume ratio equals $\frac{S}{V} = \frac{\pi d}{\frac{1}{4}\pi d^2} = \frac{4}{d}$ and $D = \frac{1}{3} v_{th} d$.[4,5] From these expressions, i.e., $\left(\frac{S}{V}\right)_{trench} = \frac{4}{2h}$, $\left(\frac{S}{V}\right)_{pore} = \frac{4}{d}$, $D_{trench} = \frac{1}{3} v_{th} \cdot 2h$ and $D_{pore} = \frac{1}{3} v_{th} \cdot d$, it is noted that the following equations that have been worked out for trench structures also hold for circular pores when replacing h by $d/2$.

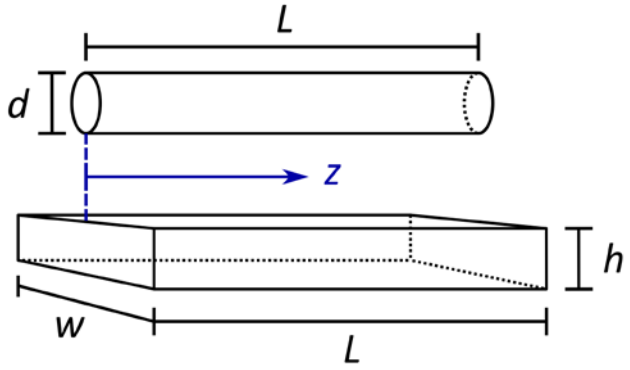

Figure S1: Geometry of a circular pore and of a trench, where z denotes the distance into the structure.

The direct relation between $\mathrm{PD}^{50\%}$ and r, derived in the main text in this work, is given by

$$\frac{\mathrm{PD}^{50\%}}{h}(t) = \frac{1}{\sqrt{\frac{3}{4}r}} \ln\left(\frac{t}{t_{50\%}}\right), \text{ where} \tag{S3}$$

$$t_{50\%} = \frac{4\ln(2)}{n_0 v_{th} A_0 s_0}\left(1 + 0.73 \cdot \frac{s_0}{r}\right). \tag{S4}$$

In this section, we show how Equation (S4) for the parameter $t_{50\%}$ has been obtained. For this, we note that Equation (S4) can be written as

$$t_{50\%} = t_{50\%,planar}(1 + f), \tag{S5}$$

where f is a dimensionless factor that has been numerically determined as $f = 0.73 \cdot \frac{s_0}{r}$ (as explained later using Figures S2 and S3), and where

$$t_{50\%,planar} = \frac{4\ln(2)}{n_0 v_{th} A_0 s_0} \tag{S6}$$

gives the dosing time needed for 50% saturation on a planar substrate where $n = n_0$. This expression for $t_{50\%,planar}$ is found by solving Equation (S2) using $\theta(0,0) = 0$ and $\lim_{t\to\infty} \theta(0,t) = 1$, giving

$$\theta(0,t) = 1 - \exp\left(-\frac{1}{4} n_0 v_{th} A_0 s_0 \cdot t\right). \tag{S7}$$

Subsequently solving $\theta\left(0, t_{50\%,planar}\right) = 1/2$, which holds by definition, then gives Equation (S6) for $t_{50\%,planar}$.

As indicated by Equation (S5), $t_{50\%,planar}$ typically cannot be used directly as the parameter $t_{50\%}$ in Equation (S3), which describes film penetration during recombination-limited growth where $\frac{r}{s_0(1-\theta)} \gg 1$. The reason for this is that, in the initial stage of the growth process, there are still many adsorption sites available (i.e., $\theta \approx 0$) near the entrance of the high-AR structure. In this stage, the loss of gas-phase radicals through adsorption reactions, described by $s_0(1-\theta)$, may still be significant or even dominant compared to the loss of radicals through surface recombination. Recombination becomes dominant when saturation is approached (i.e. $\theta \to 1$) in the entrance region that needs to be passed by the radicals to reach the growth front. As will be shown later, the factor $(1 + f)$ essentially accounts for the delay in film penetration caused by the additional loss of radicals through adsorption reactions. This is illustrated in Figure S2, where the scaled penetration depth $\mathrm{PD}^{50\%}/h$ is plotted as a function of $\ln(t)$ (a.u.), as calculated by numerically solving the full reaction-diffusion model (i.e., Equations (S1) and (S2)) for $s_0 = 10^{-4}$ and $r = 10^{-5}$.

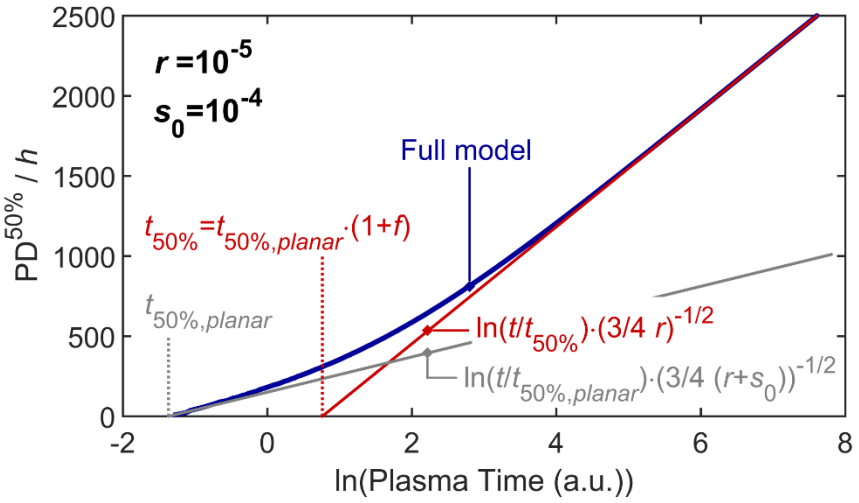

Figure S2: Scaled penetration depth $\mathrm{PD}^{50\%}/h$ plotted *against* $\ln(t)$ *(a.u.), calculated for* $r = 10^{-5}$ *and* $s_0 = 10^{-4}$ *by numerically solving the full model (Equations (S1) and (S2), blue curve) and by evaluating Equations (S3) (red line) and (S8) (gray line). The recombination-limited regime (*$t \approx 10 \cdot t_{50\%}$ *or higher) is well described by Equation (S3), where* $t_{50\%}$ *is equal to the time where the fitted line intercepts the horizontal axis.*

Figure S2 shows that the film penetration depth initially increases as

$$\frac{\mathrm{PD}^{50\%}}{h}(t) = \frac{1}{\sqrt{\frac{3}{4}(r+s_0)}} \ln\left(\frac{t}{t_{50\%,planar}}\right). \tag{S8}$$

In this stage, the surface coverage is still very low throughout the structure such that the gas-phase radical density decays according to a loss probability $r + s_0(1-\theta) \approx r + s_0$. For higher plasma exposure times, θ approaches 1 in the region where most radicals are present, such that the radical density decays less strongly according to $r + s_0(1-\theta) \approx r$ (under the assumption that r is independent on θ). As a result, the penetration depth increases more quickly with $\ln(t)$, i.e., with a slope of $1/\sqrt{\frac{3}{4}r}$ as given by Equation (S3) (note that on a linear timescale the increase in penetration depth is still slowing down). This recombination-limited regime, where the penetration depth is accurately described by Equation (S3), is approximately reached when $t > 10 \cdot t_{50\%}$. In the experiments conducted in this work, $t_{50\%} \approx 0.2$ to 0.8 s (see Figure S11) and plasma exposure times of 3.8 to 120 s were used, such that Equation (S3) could be used to determine r regardless of the value of s_0.

For the determination of the correction factor for $t_{50\%}$, we note that $t_{50\%}$ in Equation (S3) is equal to the time where $\frac{\mathrm{PD}^{50\%}}{h}(t_{50\%}) = \frac{1}{\sqrt{\frac{3}{4}r}}\ln(1) = 0$. The value of $t_{50\%}$ can therefore be determined from the intercept of the logarithmic function with the horizontal axis (see Figure S2). Due to the increase in the slope of $\mathrm{PD}^{50\%}/h$ versus ln (t), the logarithmic function describing the recombination-limited regime (red line) intercepts the horizontal axis at a time larger than $t_{50\%,planar}$. This intercept gives a fitted value of $t_{50\%}$, which has been numerically determined for a wide range and combination of values of s_0 and r (i.e., both in the range of 10^{-6} to 10^{-2}). The corresponding ratios $t_{50\%}/t_{50\%,planar}$ are plotted in Figure S3 against s_0/r. A clear linear relation is found, which is fitted as $\frac{t_{50\%}}{t_{50\%,planar}} = 1 + 0.73 \cdot \frac{s_0}{r}$. The correction factor for $t_{50\%}$ is thus given by $(1+f) = (1 + 0.73 \cdot \frac{s_0}{r})$ for all combinations of s_0 and r.

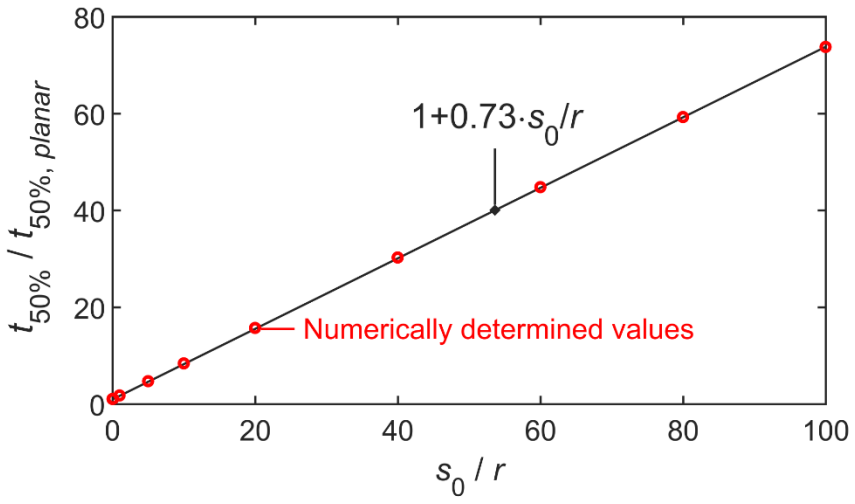

Figure S3: Ratio $t_{50\%}/t_{50\%,planar}$ plotted against s_0/r, where for each datapoint $t_{50\%,planar}$ is calculated using Equation (S6) and $t_{50\%}$ is numerically determined as illustrated in Figure S2. For all investigated values and combinations of s_0 and r, $t_{50\%}/t_{50\%,planar}$ is in good approximation equal to $1 + 0.73 \cdot s_0/r$.

MODELLING: Influence of parameters other than r

Equations (S3) and (S4) indicate that the slope of $\mathrm{PD}^{50\%}/h$ versus $\ln(t)$ is only dependent on r, which has been used in this work to experimentally determine values of r for plasma ALD of SiO_2 and TiO_2 under different process conditions. The value of $t_{50\%}$, which is determined for instance by s_0, A_0 and n_0, only shifts the data horizontally. For example, if $t_{50\%}$ would be increased by a factor a, the $\mathrm{PD}^{50\%}/h$ data would shift according to $\ln\left(\frac{t}{a \cdot t_{50\%}}\right) = \ln\left(\frac{t}{t_{50\%}}\right) - \ln(a)$. Similarly, for the slope of the function it does not matter which time unit is used (e.g. seconds or minutes).

To illustrate the effect of parameters such as s_0 and A_0, two studies are presented in Figures S4 and S5. In both figures, $\mathrm{PD}^{50\%}/h$ versus $\ln(t)$ is calculated for a surface recombination probability of $r = 5 \cdot 10^{-5}$, as determined to be typical for plasma ALD of SiO_2 and TiO_2. An absolute timescale is given in ln(seconds), where the absolute values depend on the product $\frac{1}{4} n_0 v_{th} A_0$ (s^{-1}). This product describes the number of gas-phase radicals hitting the surface per second per adsorption site. For typical conditions, $\frac{1}{4} n_0 v_{th} A_0$ is expected to lie in the range of 10^3 up to 10^6 s^{-1}.

In Figure S4, s_0 is varied from 10^{-6} up to 10^{-2} while keeping all other parameters constant, with $\frac{1}{4} n_0 v_{th} A_0 = 5 \cdot 10^4$ s^{-1}. It is observed that, for higher values of s_0, the $\mathrm{PD}^{50\%}/h$ curves shift to lower plasma times up to the point where $t_{50\%}$ (i.e., the intercept of the dotted lines with the horizontal axis, calculated using Equation (S4)) reaches a lower limit of $t_{50\%} \approx \frac{4 \ln(2) 0.73}{n_0 v_{th} A_0 r}$ when $0.73 \cdot \frac{s_0}{r} \gg 1$. In the other direction, the curves start to shift linearly with s_0 when $s_0 \ll r$, since in that regime $t_{50\%} \approx \frac{4 \ln(2)}{n_0 v_{th} A_0 s_0}$. Moreover, when $s_0 \ll r$, Equation (S3) (dotted lines) is also accurate in the initial stage of the growth process where $t < 10 \cdot t_{50\%}$.

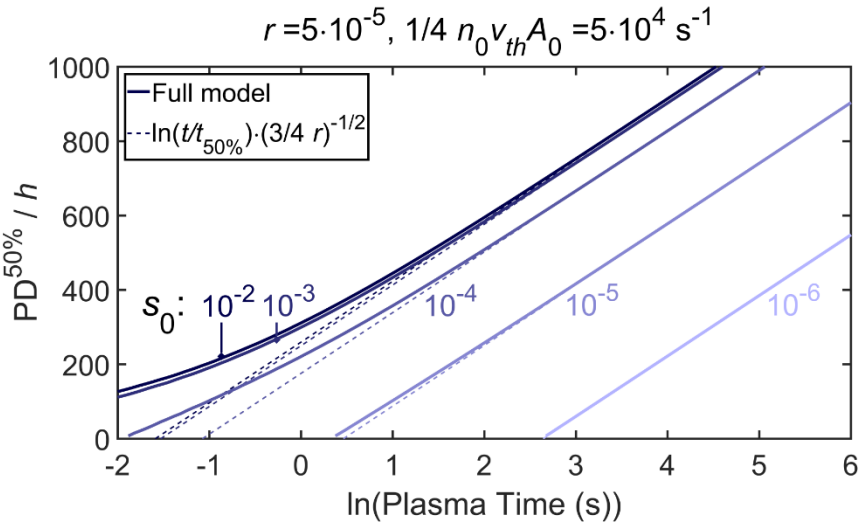

Figure S4: Scaled penetration depth $\mathrm{PD}^{50\%}/h$ plotted *against* $\ln(t)$ *(in seconds), calculated for* $r = 5 \cdot 10^{-5}$, $\frac{1}{4} n_0 v_{th} A_0 = 5 \cdot 10^4$ s^{-1} *and varied values of* s_0. *For higher values of* s_0 *film growth is achieved within shorter plasma steps, up to a lower limit that is determined by* r *and* $\frac{1}{4} n_0 v_{th} A_0$ *(see Equation (S4)). The slope of the curves in the recombination-limited growth regime is unaffected, such that Equation (S3) (corresponding to the dotted lines) can be used to determine* r *regardless of the value of* s_0.

Similarly, in Figure S5 the product $\frac{1}{4}n_0 v_{th} A_0$ is varied from 10^3 to 10^6 s^{-1} while keeping $r = 5 \cdot 10^{-5}$ and $s_0 = 10^{-4}$ constant. It is observed that the curves shift linearly with $\frac{1}{4}n_0 v_{th} A_0$, where a given film penetration is reached within shorter plasma steps when $\frac{1}{4}n_0 v_{th} A_0$ is higher (i.e., when having a higher flux of radicals and/or less adsorption sites per unit area). The accuracy of Equation (S3) (dotted lines) is not influenced by $\frac{1}{4}n_0 v_{th} A_0$.

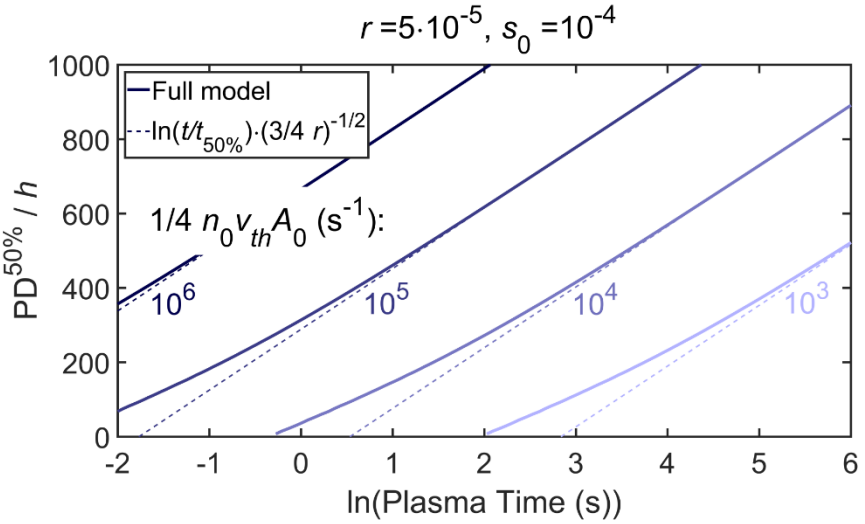

Figure S5: Scaled penetration depth $\mathrm{PD}^{50\%}/h$ plotted *against* $\ln(t)$ *(in seconds), calculated for* $r = 5 \cdot 10^{-5}$, $s_0 \cdot 10^{-4}$ *s*$^{-1}$ *and varied values of* $\frac{1}{4}n_0 v_{th} A_0$ *(s*$^{-1}$*). For higher values of* $\frac{1}{4}n_0 v_{th} A_0$ *film growth is achieved within shorter plasma steps, while the slope of the curves is unaffected.*

The examples given in Figures S4 and S5 illustrate that parameters that could be dependent on the precursor, such as the number of adsorption sites per unit surface area ($1/A_0$), do not influence the slope of $\mathrm{PD}^{50\%}/h$ versus $\ln(t)$ and thus the determination of r. The used precursor could influence the value of r itself, but only when the properties of the saturated surface during plasma exposure (e.g., any residual hydrogen and carbon content) depend on the precursor. This is because the value of r determined in our method corresponds to the saturated surface for plasma exposure, while the value of r corresponding to the precursor-terminated surface is expected to play a minor role. To illustrate this, Figure S6 gives $\mathrm{PD}^{50\%}/h$ curves that are calculated using a coverage-dependent recombination probability, where

$$r = r_{\theta=0} \cdot (1 - \theta) + r_{\theta=1} \cdot \theta. \qquad \text{(S9)}$$

Such a coverage-dependent recombination probability has been observed for instance for ozone during ALD of ZnO, where the value of r was lower on the precursor-terminated surface ($\theta = 0$).[6]

In Figure S6, the value of r corresponding to the saturated surface ($\theta = 1$) is the same as in Figures S4 and S5, namely $r_{\theta=1} = 5 \cdot 10^{-5}$, while the value of $r_{\theta=0}$ is varied from $5 \cdot 10^{-7}$ to $5 \cdot 10^{-4}$. To clearly illustrate the influence of a coverage-dependent recombination probability, the value of $s_0 = 10^{-5}$ is chosen to be lower than $r_{\theta=1}$. When $r_{\theta=0}$ is lower than $r_{\theta=1}$, for example when $r_{\theta=0}/r_{\theta=1} = 0.01$ or 0.1, it is observed that film growth propagates relatively rapidly in the initial stage and slows down when $\mathrm{PD}^{50\%}/h \approx \ln(10) / \sqrt{\frac{3}{4}\, r_{\theta=1}}$ or higher. At that point, most radicals recombine on the saturated surface, such that $r_{\theta=1}$ becomes dominant. The other way around, film penetration is delayed when $r_{\theta=0}$ is higher than $r_{\theta=1}$, but in all cases the slope of $\mathrm{PD}^{50\%}/h$ versus $\ln(t)$ is eventually only determined by the value of $r_{\theta=1}$. The value of $r_{\theta=1}$ (corresponding to the saturated surface) is therefore determined in our method, which is expected to be relatively independent of the used precursor.

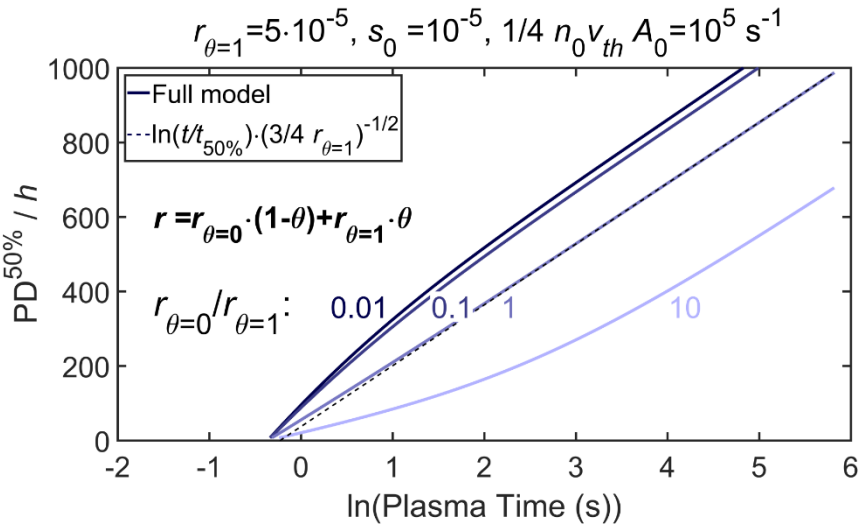

Figure S6: Scaled penetration depth $\mathrm{PD}^{50\%}/h$ plotted *against* $\ln(t)$ *(in seconds), calculated using a coverage-dependent value of* r*, where* $r(\theta = 1) = r_{\theta=1} = 5 \cdot 10^{-5}$ *is the same as in Figures S4 and S5. The initial value of* r *can accelerate* ($r_{\theta=0} < r_{\theta=1}$) *or delay* ($r_{\theta=0} > r_{\theta=1}$) *film penetration, but the eventual slope of the curves is only determined by the value of* r *corresponding to the saturated surface.*

Finally, it should be noted that, while the value of s_0 does not influence the determination of r, it does influence the shape of the coverage profile (and consequently the thickness profile). This is illustrated in Figure S7. For higher values of s_0, the radicals are more likely to react (e.g., participate in ligand removal) directly at the profile front where unreacted adsorption sites are still available. As a consequence, the profile becomes sharper for higher values of s_0.[7]

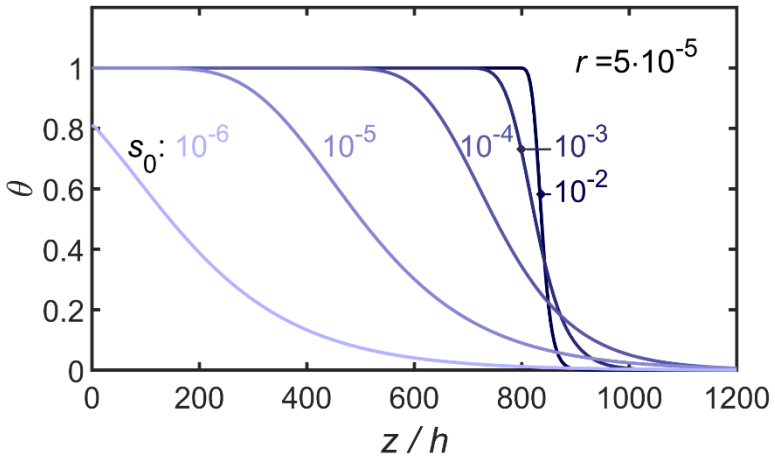

Figure S7: Coverage profiles for various values of s_0, a fixed value of $r = 5 \cdot 10^{-5}$, and a plasma time of 34 s with $\frac{1}{4} n_0 v_{th} A_0 = 5 \cdot 10^4$ s^{-1}. For higher values of s_0, the profile front becomes sharper and the film penetrates deeper, up to a limit that is determined by r, t and $\frac{1}{4} n_0 v_{th} A_0$ (see Equations (S3) and (S4)).

The shape of the coverage profile thus contains information on the value of s_0. For example, the thickness profiles measured in this work (see Figures S9 and S10) are best described using an s_0 of 10^{-5} to 10^{-3}. However, the profile also becomes sharper for higher values of r (see Figure S8), which is caused by a more rapid decay in radical density. This makes it difficult to accurately determine an effective value of s_0. Finally, Figure S8 also illustrates that the value of r has a dominant impact on the film penetration depth, making it a key parameter for optimizing film conformality during plasma ALD on high-AR structures.

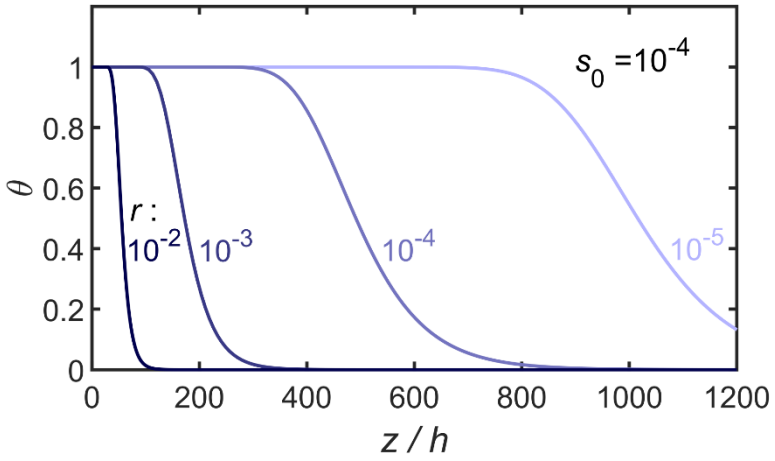

Figure S8: Coverage profiles for various values of r, a fixed value of $s_0 = 10^{-4}$, and a plasma time of 17 s with $\frac{1}{4} n_0 v_{th} A_0 = 5 \cdot 10^4$ s^{-1}. For higher values of r, the profile front becomes sharper and the penetration depth of the film strongly reduces (see Equation (S3)).

EXPERIMENTAL: Measured thickness profiles at different plasma exposure times

The values of r and $t_{50\%}$ reported in this work were determined by measuring the thickness profiles of SiO_2 and TiO_2 films deposited into lateral-high-aspect-ratio (LHAR) trench structures, using different plasma exposure times. An overview of these thickness profiles is given below, for the different temperature setpoints (Figure S9) and plasma pressures (Figure S10) investigated. The distance at which the thickness has decreased to 50% of its value at the entrance of the LHAR structure corresponds to the half-thickness-penetration-depth $PD^{50\%}$. The measured values of $PD^{50\%}/h$, where h is the cavity height of the LHAR structure, are provided in the main article and have been used to calculate the values of r and $t_{50\%}$.

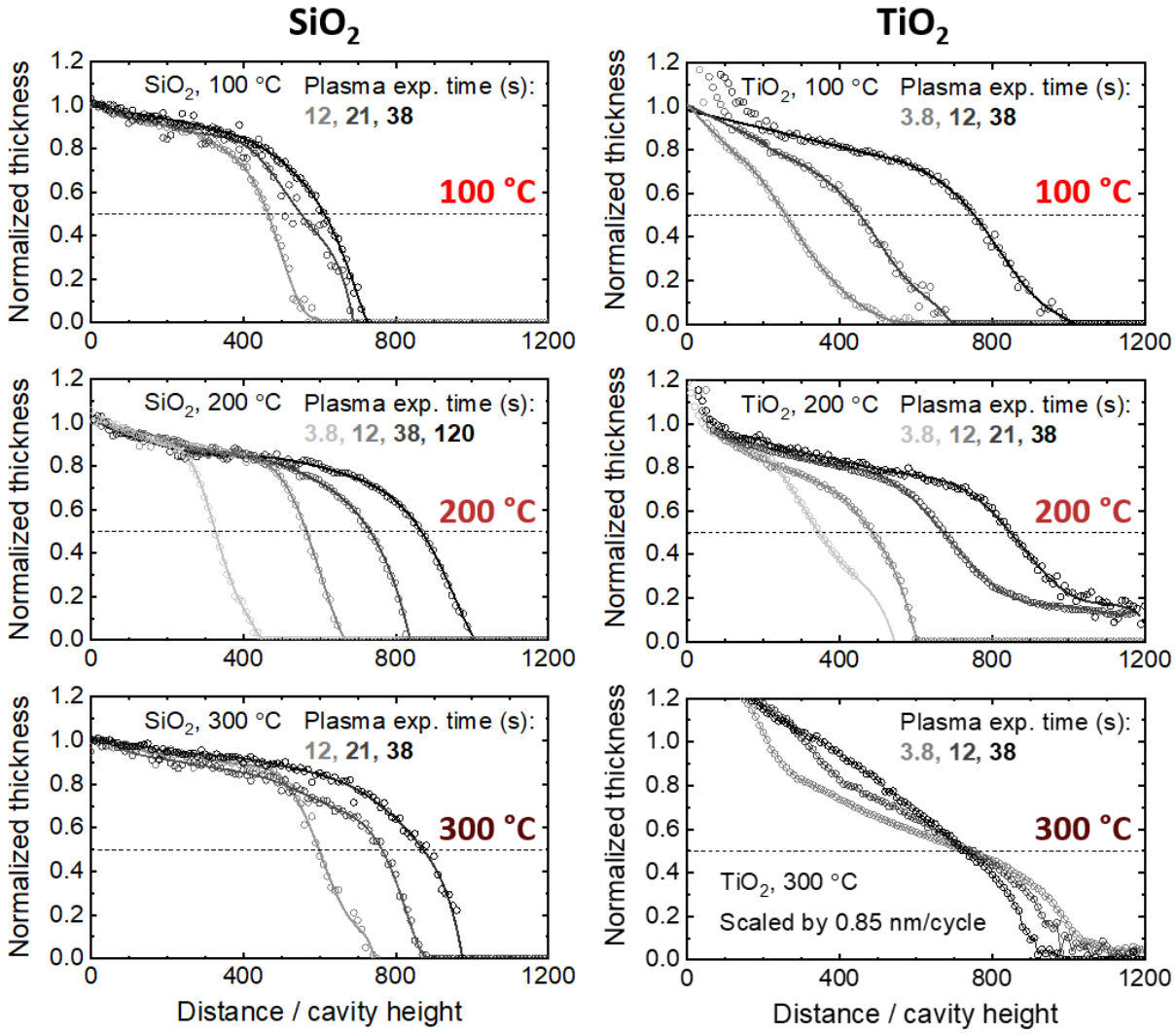

Figure S9: Normalized thickness profiles of SiO_2 and TiO_2 films grown by plasma ALD on LHAR cavity structures, using 50 mTorr plasma pressure, temperature setpoints of 100, 200 or 300 ℃ and plasma exposure times of 3.8, 12, 21, 38 or 120 seconds per cycle.

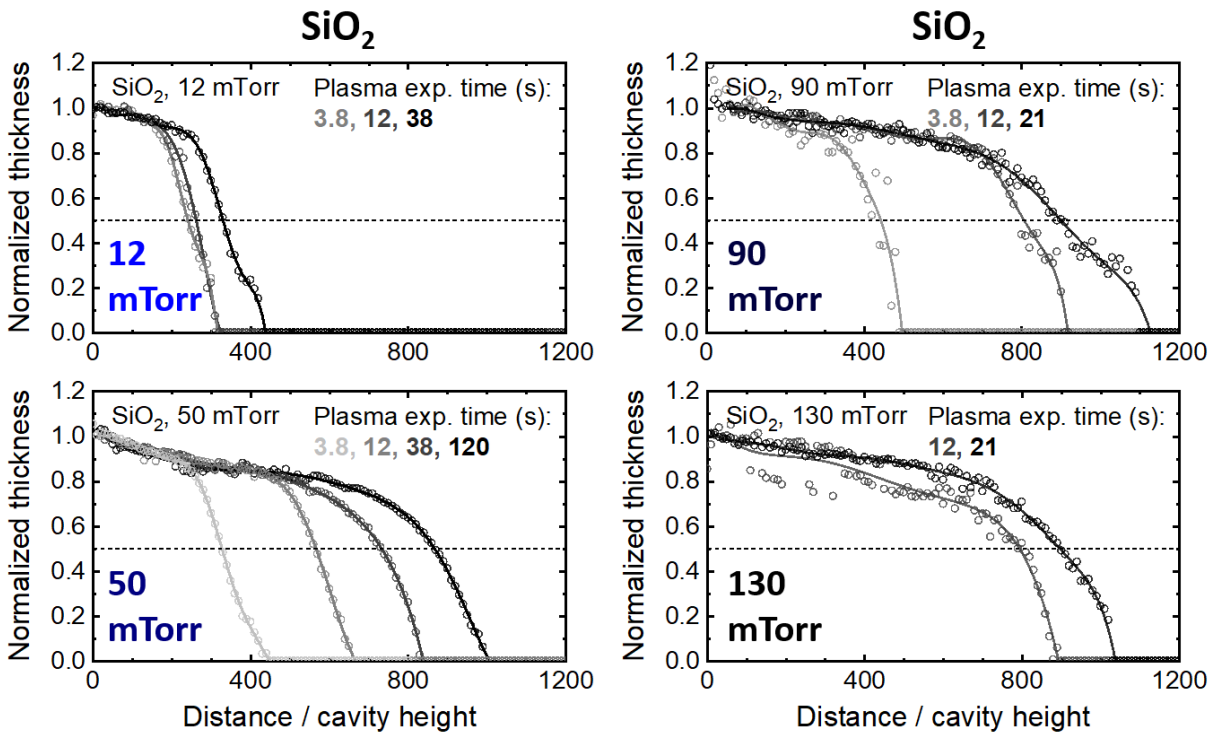

Figure S10: Normalized thickness profiles of SiO_2 films grown by plasma ALD on LHAR cavity structures, using a temperature setpoint of 200 °C, plasma pressures of 12, 50 or 90 or 130 mTorr and plasma exposure times of 3.8, 12, 21, 38 or 120 seconds per cycle.

EXPERIMENTAL: Determined values of r and $t_{50\%}$

In Table S1, we provide an overview of the values of r and $t_{50\%}$ that are determined using the $PD^{50\%}/h$ data corresponding to the thickness profiles plotted in Figures S9 and S10. The values of r and $t_{50\%}$ combined have been used to calculate the saturation times t_{sat} for trenches with different ARs (see Equation (S18) later in this document). To graphically illustrate the influence of substrate temperature and plasma pressure, the determined values of $t_{50\%}$ are also plotted in Figure S11.

Table S1: Values of r and $t_{50\%}$ determined for plasma ALD of SiO_2 and TiO_2 at different substrate temperatures and plasma pressures. The substrate temperatures of 100, 180 and 240 ℃ correspond to table temperature setpoints of 100, 200 and 300 ℃ and have an uncertainty of approximately 15 ℃. The plasma pressure has an uncertainty of approximately 5 mTorr.

Material	Substrate temperature (℃)	Plasma pressure (mTorr)	$r \times 10^5$		$t_{50\%}$ (s)	
			Best fit	Uncertainty range	Best fit	Uncertainty range
SiO_2	100	50	9	5-23	0.22	0.11-0.32
SiO_2	180	50	6	5-8	0.26	0.19-0.34
SiO_2	240	50	3	2-5	0.71	0.38-1.03
TiO_2	100	50	4	3-6	0.80	0.45-1.15
TiO_2	180	50	4	2-5	0.57	0.20-0.95
TiO_2	240	50	<1			
SiO_2	180	12	24	7-70	0.49	0.1-1
SiO_2	180	50	6	5-8	0.26	0.19-0.34
SiO_2	180	90	2.3	1.8-2.8	0.43	0.29-0.57
SiO_2	180	130	2	1-6	0.43	0.1-1

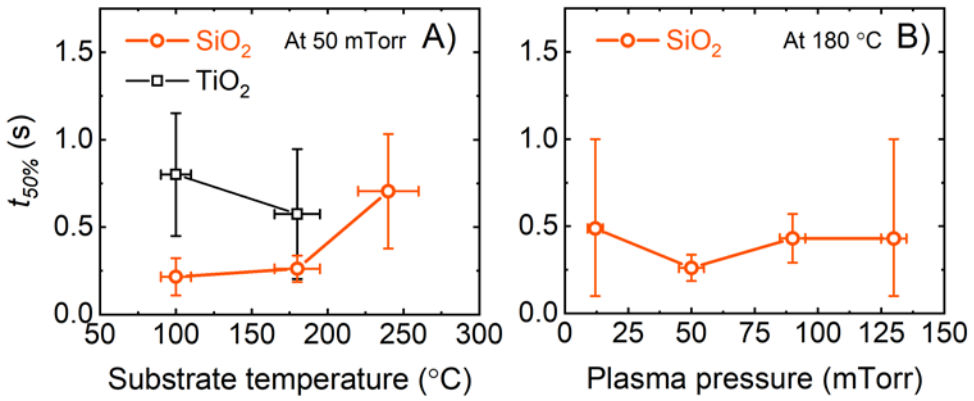

Figure S11: Determined values of $t_{50\%}$ for the SiO_2 and TiO_2 depositions carried out at different substrate temperatures (A), and for the SiO_2 depositions carried out at different plasma pressures (B).

EXPERIMENTAL: Calculation of the given uncertainties

- **Uncertainties of r and $t_{50\%}$**

In this section, we describe how the uncertainties of the reported values of r, $t_{50\%}$ and t_{sat} have been calculated. For this, we first note that the values of r and $t_{50\%}$ have been determined by fitting the $\mathrm{PD}^{50\%}/h$ data using a linear function $y = ax + b$, where each datapoint i has a coordinate (x_i, y_i) given by

$$x_i = \ln(t_i), \text{ and} \tag{S10}$$

$$y_i = \mathrm{PD}_i^{50\%}/h. \tag{S11}$$

The coefficients a and b of the linear fits have been calculated using the least squares method, where

$$a = \frac{N\Sigma x_i y_i - \Sigma x_i \Sigma y_i}{N\Sigma x_i^2 - (\Sigma x_i)^2}, \tag{S12}$$

$$b = \frac{\Sigma x_i^2 \Sigma y_i - \Sigma x_i \Sigma x_i y_i}{N\Sigma x_i^2 - (\Sigma x_i)^2}, \tag{S13}$$

and N is the number of datapoints. Subsequently, the values of r and $t_{50\%}$ follow directly from the values of a and b. This is because $a = \frac{1}{\sqrt{\frac{3}{4r}}}$ and $a\ln(t_{50\%}) + b = 0$ (see Equation (S3)), such that

$$r = \frac{4}{3a^2}, \text{ and} \tag{S14}$$

$$t_{50\%} = \exp\left(-\frac{b}{a}\right). \tag{S15}$$

The reported uncertainties of r and $t_{50\%}$ are based on the uncertainties S_a and S_b of the fitted coefficients a and b, which are calculated as

$$S_a = \sqrt{\frac{NS_y}{N\Sigma x_i^2 - (\Sigma x_i)^2}}, \text{ and} \tag{S16}$$

$$S_b = \sqrt{\frac{S_y^2 \Sigma x_i^2}{N\Sigma x_i^2 - (\Sigma x_i)^2}}. \tag{S17}$$

Here, S_y denotes the uncertainty of the y values, so of the values of $\mathrm{PD}^{50\%}/h$. In this work, the uncertainty of $\mathrm{PD}^{50\%}/h$ was mainly governed by the width of the front of the measured thickness profile, where a sharp front gives a more accurate value of $\mathrm{PD}^{50\%}/h$. For the SiO_2 data, the uncertainty of $\mathrm{PD}^{50\%}/h$ has been estimated as $S_y = 40$ and for the TiO_2 data as $S_y = 60$.

- **Uncertainty of calculated saturation times t_{sat}**

The plasma exposure time needed to reach saturation on a high-AR structure, called t_{sat}, was calculated as

$$t_{sat} \approx t_{50\%} \exp\left(\sqrt{\frac{3}{4}r}\mathrm{AR}\right). \tag{S18}$$

The uncertainty in t_{sat} can therefore be calculated using the aforementioned uncertainties in $t_{50\%}$ and r. For instance, a minimum or maximum value of t_{sat} could be estimated using the minimum or maximum values of $t_{50\%}$ and r within their uncertainty intervals. However, in this way the uncertainty in t_{sat} is strongly overestimated, since the uncertainties of $t_{50\%}$ and r are not independent. For example, for a lower value of $t_{50\%}$ the measured $\mathrm{PD}^{50\%}/h$ data can only be described using a higher value of r, and vice versa. A more representative uncertainty range of t_{sat} has been calculated using a potential systematic measurement offset Δy in the linear function $y = ax + b$ fitted through the $\mathrm{PD}^{50\%}/h$ data. This potential offset has been estimated as

$$\Delta y = \left(\frac{1}{\sqrt{\frac{3}{4}r}}\ln\left(\frac{t}{t_{50\%,min}}\right) - \frac{1}{\sqrt{\frac{3}{4}r}}\ln\left(\frac{t}{t_{50\%,max}}\right)\right)$$

$$= \frac{1}{\sqrt{\frac{3}{4}r}}\frac{\ln(t_{50\%,max}) - \ln(t_{50\%,min})}{2}, \tag{S19}$$

where $t_{50\%,min}$ and $t_{50\%,max}$ are the minimum and maximum values of $t_{50\%}$ within its uncertainty interval. In our model, the saturation time t_{sat} corresponds to the time where $y = \frac{\mathrm{PD}^{50\%}}{h}(t) = \mathrm{AR}$. Therefore, an offset Δy increases or reduces the saturation time according to

$$t_{sat,min} = t_{50\%} \exp\left(\sqrt{\frac{3}{4}r}(\mathrm{AR} - \Delta y)^2\right), \text{ and} \tag{S20}$$

$$t_{sat,max} = t_{50\%} \exp\left(\sqrt{\frac{3}{4}r}(\mathrm{AR} + \Delta y)^2\right). \tag{S21}$$

Equations (S20) and (S21) have thus been used to calculate the upper limits ($t_{sat,max}$) and lower limits ($t_{sat,min}$) of the values of t_{sat} reported in this work.

EXPERIMENTAL: Details TEM image

In the fabrication of semiconductor logic and memory devices, plasma ALD of SiO_2 and TiO_2 have been reported to be used for gap-filling of electrical isolation regions.[8–10] The challenging nature of gap-filling was demonstrated in the introduction of this work, using a cross-sectional transmission electron microscope (TEM) image of a SiO_2 film grown by plasma ALD on vertically-oriented trench nanostructures. Here, we provide additional experimental information on the provided TEM image.

First of all, the coupon containing the vertical trench structures, having different aspect ratios in the range of approximately 1 to 10,[11,12] was prepared and provided by Lam Research. The TEM image of the structures was measured using a JEOL ARM 200F TEM in bright-field mode (BF-TEM). For this, the processed coupon was protected by a spin-on epoxy layer and the TEM sample was subsequently prepared by a standard focused ion beam (FIB) lift-out scheme. The displayed SiO_2 film was grown by $SiH_2(NEt_2)_2$ and O_2 plasma, using 250 ALD cycles. For the purpose of visualizing the starting surface, first a ~5 nm thick layer of Al_2O_3 was grown by $Al(CH_3)_3$ and H_2O, using 50 ALD cycles. Both films were deposited at a temperature setpoint of 200 ℃, using a FlexAL ALD tool of Oxford Instruments. The O_2 plasma half-cycles were carried out using 15 mTorr plasma pressure, 200 W ICP power, 5 s plasma exposure, and 15 W substrate biasing, giving a high mean ion energy of approximately 130 eV.[13] These plasma conditions were not optimized for achieving a high film conformality. Specifically, for plasma ALD of SiO_2 the GPC reduces under the influence of ions,[11,14] which mostly affects the growth on surfaces undergoing ion impingement (e.g., the planar bottom and top surfaces rather than the vertical sidewalls).[11] This effect was relatively pronounced in this case study, because of the high ion energy dose provided.[14] Nevertheless, a seamless gap-fill was still observed, similar to depositions done without substrate biasing.

References

(1) Yanguas-Gil, A.; Elam, J. W. Self-Limited Reaction-Diffusion in Nanostructured Substrates: Surface Coverage Dynamics and Analytic Approximations to ALD Saturation Times. *Chem. Vap. Depos.* **2012**, *18* (1–3), 46–52. https://doi.org/10.1002/cvde.201106938.

(2) Arts, K.; Utriainen, M.; Puurunen, R. L.; Kessels, W. M. M.; Knoops, H. C. M. Film Conformality and Extracted Recombination Probabilities of O Atoms during Plasma-Assisted Atomic Layer Deposition of SiO2, TiO2, Al2O3, and HfO2. *J. Phys. Chem. C* **2019**, *123* (44), 27030–27035. https://doi.org/10.1021/acs.jpcc.9b08176.

(3) Ylilammi, M.; Ylivaara, O. M. E.; Puurunen, R. L. Modeling Growth Kinetics of Thin Films Made by Atomic Layer Deposition in Lateral High-Aspect-Ratio Structures. *J. Appl. Phys.* **2018**, *123*, 205301. https://doi.org/10.1063/1.5028178.

(4) O'Hanlon, J. F. *A User's Guide to Vacuum Technology*; Wiley: New Jersey, 2003.

https://doi.org/10.1002/0471467162.

(5) Poodt, P.; Mameli, A.; Schulpen, J.; Kessels, W. M. M. (Erwin); Roozeboom, F. Effect of Reactor Pressure on the Conformal Coating inside Porous Substrates by Atomic Layer Deposition. *J. Vac. Sci. Technol. A Vacuum, Surfaces, Film.* **2017**, *35* (2), 021502. https://doi.org/10.1116/1.4973350.

(6) Knoops, H. C. M.; Elam, J. W.; Libera, J. A.; Kessels, W. M. M. Surface Loss in Ozone-Based Atomic Layer Deposition Processes. *Chem. Mater.* **2011**, *23* (9), 2381–2387. https://doi.org/10.1021/cm2001144.

(7) Arts, K.; Vandalon, V.; Puurunen, R. L.; Utriainen, M.; Gao, F.; Kessels, W. M. M.; Knoops, H. C. M. Sticking Probabilities of H2O and Al(CH3)3 during Atomic Layer Deposition of Al2O3 Extracted from Their Impact on Film Conformality. *J. Vac. Sci. Technol. A* **2019**, *37* (3), 030908. https://doi.org/10.1116/1.5093620.

(8) ASM International Analyst and Investor Technology Seminar, presented at Semicon West, July 9, 2019. https://www.asm.com/Downloads/ASMI Analyst and Investor Technology Seminar July 9 2019 revREL.PDF.

(9) Tang, W.; Park, J. D.; Schravendijk, B. Van; Ashtiani, K. US 9.406,544 B1 - Systems and Methods for Eliminating Seams in Atomic Layer Deposition of Silicon Dioxide Film in Gap Fill Applications. *United States Pat.* **2016**.

(10) Swaminathan, S.; Pasquale, F. L.; LaVoie, A. US 9,373,500 B2 - Plasma Assisted Atomic Layer Deposition Titanium Oxide for Conformal Encapsulation and Gapfill Applications. *United States Pat.* **2016**.

(11) Faraz, T.; Knoops, H. C. M.; Verheijen, M. A.; van Helvoirt, C. A. A.; Karwal, S.; Sharma, A.; Beladiya, V.; Szeghalmi, A.; Hausmann, D. M.; Henri, J.; et al. Tuning Material Properties of Oxides and Nitrides by Substrate Biasing during Plasma-Enhanced Atomic Layer Deposition on Planar and 3D Substrate Topographies. *ACS Appl. Mater. Interfaces* **2018**, *10*, 13158–13180. https://doi.org/10.1021/acsami.8b00183.

(12) Sharma, A.; Longo, V.; Verheijen, M. A.; Bol, A. A.; Kessels, W. M. M. (Erwin). Atomic Layer Deposition of HfO2 Using HfCp(NMe2)3 and O2 Plasma. *J. Vac. Sci. Technol. A Vacuum, Surfaces, Film.* **2017**, *35* (1), 01B130. https://doi.org/10.1116/1.4972210.

(13) Faraz, T.; Arts, K.; Karwal, S.; Knoops, H. C. M.; Kessels, W. M. M. Energetic Ions during Plasma-Enhanced Atomic Layer Deposition and Their Role in Tailoring Material Properties. *Plasma Sources Sci. Technol.* **2019**, *28* (2), 024002. https://doi.org/10.1088/1361-6595/aaf2c7.

(14) Arts, K.; Deijkers, J. H.; Faraz, T.; Puurunen, R. L.; Kessels, W. M. M.; Knoops, H. C. M. Evidence for Low-Energy Ions Influencing Plasma-Assisted Atomic Layer Deposition of SiO2: Impact on the Growth per Cycle and Wet Etch Rate. *Appl. Phys. Lett.* **2020**, *117*, 031602. https://doi.org/10.1063/5.0015379.